Research Article Vol. 3, No. 1 / January 2016 / Optica 64

Large-scale broadband digital silicon photonic switches with vertical adiabatic couplers

Tae Joon Seok,[1] Niels Quack,[2] Sangyoon Han,[1] Richard S. Muller,[1] and Ming C. Wu[1,*]

[1]Department of Electrical Engineering and Computer Sciences, University of California, Berkeley, California 94720, USA
[2]École Polytechnique Fédérale de Lausanne (EPFL), CH-1015 Lausanne, Switzerland
*Corresponding author: wu@eecs.berkeley.edu

Received 19 October 2015; revised 4 December 2015; accepted 7 December 2015 (Doc. ID 252161); published 13 January 2016

Large-scale photonic switches are essential devices for energy- and cost-efficient optical communication networks in cloud and data-intensive computing. Silicon photonics is an attractive platform for high-density photonic integrated circuits with low manufacturing costs through the leveraging of existing advanced complementary metal-oxide-semiconductor processes. Many optical components such as lasers, modulators, splitters, and photodetectors have been successfully integrated on silicon; however, the quest for large-scale silicon photonic switches has remained elusive. Previous silicon photonic switches made of cascaded 1 × 2 or 2 × 2 building blocks have a limited port count (≤8 × 8) or excessive optical losses (>15 dB). Here, we present a 64 × 64 digital silicon photonic switch with a low on-chip insertion loss (3.7 dB) and broadband operation (300 nm). The measured switching time is 0.91 μs, and the extinction ratio is larger than 60 dB. The matrix switch with 4096 microelectromechanical-systems-actuated vertical adiabatic couplers has been integrated on a 8.6 mm × 8.6 mm chip. To our knowledge this is the largest monolithic switch, and the largest silicon photonic integrated circuit, reported to date. The passive matrix architecture of our switch is fundamentally more scalable than that of multistage switches.

OCIS codes: (130.4815) Optical switching devices; (250.5300) Photonic integrated circuits.

http://dx.doi.org/10.1364/OPTICA.3.000064

1. INTRODUCTION

The advent of cloud and data-intensive computing has created a need for large-scale photonic switches [1–7]. Silicon photonics has emerged as a powerful platform for high-density photonic integrated circuits because complex photonic circuits with a large number of components can be monolithically integrated at low cost and with high yield by leveraging an advanced complementary metal-oxide-semiconductor manufacturing process [8–12]. In the past few years, several silicon photonic switches have been reported [13–18]. They have a nearly 50-fold higher integration density than silica-based planar lightwave circuits [19]. However, they are limited in scale (≤8 × 8) [18,20,21] or have excessive losses (>15 dB) [22], because (1) they use inefficient electro-optic (free carrier) or thermo-optic switching mechanisms, and (2) they incur high cumulative losses in cascaded 1 × 2 or 2 × 2 switching blocks in multistage switches. Electro-optic or thermo-optic effects on silicon introduce a small change in the refractive index (<10%) and must be embedded in Mach–Zehnder interferometers (MZIs) or ring resonators to achieve switching. The MZIs have non-negligible losses for both switching states, while the ring resonators have a very narrow optical bandwidth. Previously, we reported a microelectromechanical systems (MEMS)-actuated matrix switch that scales to 50 × 50 ports [23]; however, it employs directional couplers that limit the optical bandwidth to 20 nm. The analog actuation mechanism also requires precise control of the switching voltage (to within 100 mV).

In this paper, we present a broadband digital silicon photonic switch that employs two-layer waveguides and MEMS-actuated vertical adiabatic couplers. The adiabatic coupler operates over a broad optical bandwidth (1400–1700 nm), making it fully compatible with wavelength-division multiplexing networks. The digital switching operation eliminates bias-dependent losses without requiring feedback control. These couplers also eliminate optical losses in the OFF state, allowing us to take full advantage of the matrix architecture. Optical signals pass through only one active switching cell along the light path, eliminating the cumulative losses. Experimentally, we have designed and fabricated a 64 × 64 digital switch with a record low (to our knowledge) on-chip loss of 3.7 dB. The loss-to-port-count ratio of 0.058 dB/port is 10× lower than all other Si photonic switches [20–23] that we are aware of. The compact silicon photonic MEMS device has a switching time of only 0.91 μs, 1000× faster than conventional 3D MEMS switches [24,25].

2. SWITCH DESIGN

The schematic of our switch architecture is shown in Figs. 1(a) and 1(b). It is a strictly nonblocking matrix architecture consisting of two orthogonal sets of bus waveguides and low-loss crossings at intersections. The switch we reported previously has high optical

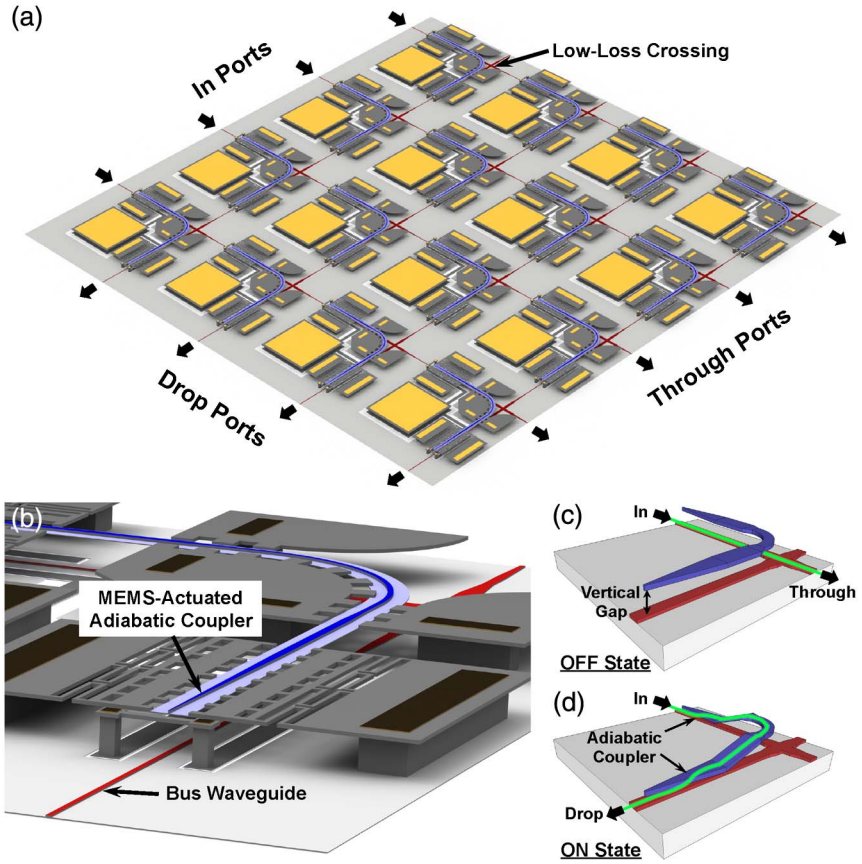

Fig. 1. Schematics of silicon photonic MEMS switches. (a) Matrix architecture of silicon photonic MEMS switch, (b) close-up view of a MEMS-actuated adiabatic coupler, (c) switch unit cell in the OFF state, and (d) switch unit cell in the ON state. The adiabatic coupler is precisely positioned at the optimum distance to the bus waveguide.

loss (27.5 dB) due to a fundamental trade-off between waveguide width (loss) and switch efficiency in lateral directional couplers [23]. In our new design, we use vertical couplers to overcome this trade-off. The switching element consists of a pair of MEMS-actuated vertical adiabatic couplers. The vertical adiabatic couplers offer many advantages over lateral directional couplers. First, because we can control the coupling gap precisely with mechanical stoppers, strong coupling can be achieved over a short coupling length. This allows us to reduce the footprint of the switch. Second, the coupling strength is independent of the waveguide width. This enables us to use wide rib waveguides that have much lower loss than narrow strip waveguides. Third, the adiabatic couplers can be easily implemented by tapering the waveguide width lithographically. The adiabatic couplers offer broadband operation (over 300 nm wavelength range) and robust fabrication tolerances.

Figures 1(c) and 1(d) illustrate the switching operations in the OFF and ON states, respectively. In the OFF state, the adiabatic couplers are located far above the bus waveguides (1 μm), so light continues to propagate toward the through port without interruption, as shown in Fig. 1(c). In the ON state, the adiabatic couplers are physically moved toward the bus waveguide by MEMS electrostatic gap-closing actuators [Fig. 1(d)]. Light is efficiently coupled to the upper waveguide. After a 90-degree bend, light is coupled to an orthogonal bus waveguide through another adiabatic coupler and propagates to the drop port. Low optical loss is achieved because light travels through only one switching element along the optical path. The detailed design of the MEMS actuators is described in Section I of Supplement 1.

The bus waveguides are implemented on 220 nm thick silicon-on-insulator wafers with 3 μm thick buried oxide layers. Rib waveguides with 60 nm ridge heights and 600 nm widths are used for low propagation loss. The insertion loss of waveguide crossings is substantially reduced to 0.011 dB by multimode interference (MMI) focusing structures (Section II of Supplement 1). The schematic of the adiabatic coupler is shown in Fig. 2(a). We use fine-grained polycrystalline silicon (polysilicon) for both the coupler waveguide and the MEMS actuators. The coupler waveguide has a ridge structure with a core thickness of 300 nm and a ridge height of 200 nm. The coupler width is tapered from 150 nm to 1 μm over a length of 30 μm, while the width of the bus waveguide remains constant at 600 nm. The performance of the adiabatic couplers is simulated numerically using a time-domain solver. Figure 2(b) shows the calculated effective refractive indices of the optical modes in the coupled waveguides with 125 nm spacing. Mode 1 (red line) in the plot clearly shows that the optical mode of the bus waveguide at the input port (distance = 0 μm) is adiabatically transferred to the mode of the coupler waveguide at the output port (distance = 30 μm). The optical mode profiles at several locations along the coupler are shown in Fig. 2(c). It is challenging to switch the light path from this adiabatic coupler by a small refractive index change of the silicon electro-optic or thermo-optic effect. Therefore, we change the gap spacing between the bus and coupler waveguides by MEMS actuation to achieve the

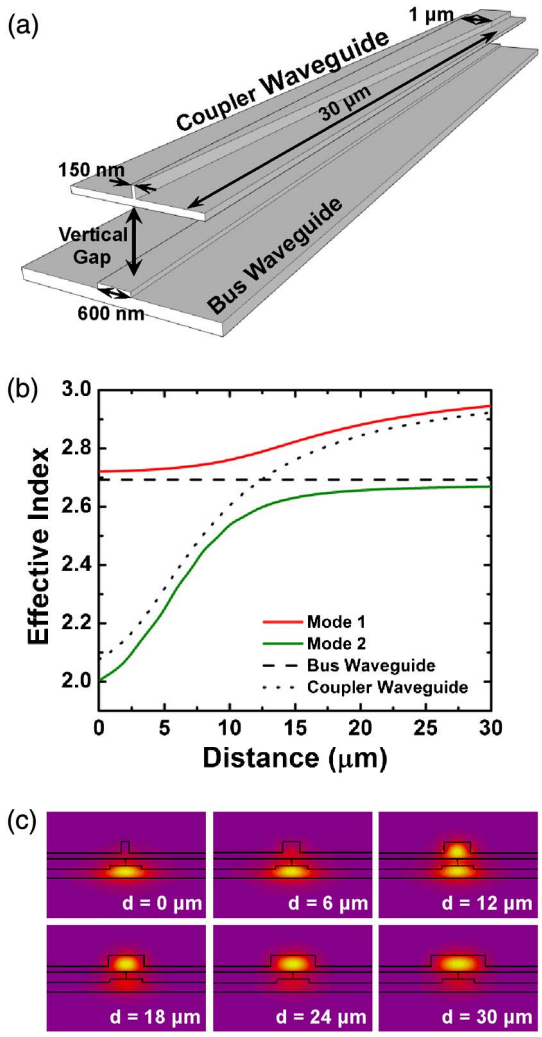

Fig. 2. Numerical simulations of the adiabatic directional coupler. (a) Schematic of the simulated structure. The ridge width of the adiabatic coupler is tapered from 150 nm to 1 μm over a 30 μm length. (b) Effective refractive index calculation of adiabatic coupler modes. The gap spacing between two waveguides is 125 nm. Dashed and dotted lines represent the individual effective refractive indices of the bus waveguide and coupler waveguide, respectively. (c) Field profile of bus waveguide and adiabatic coupler at 0, 6, 12, 18, 24, and 30 μm distances (Gap = 125 nm).

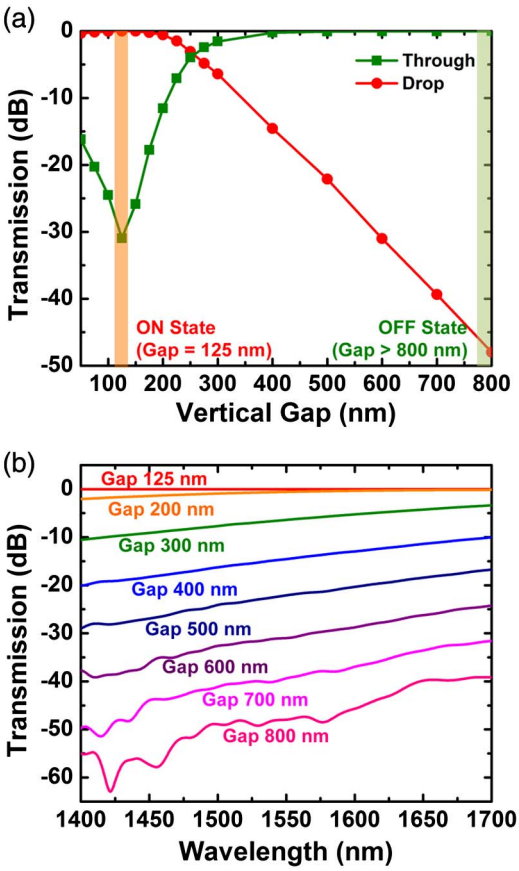

Fig. 3. Simulated transfer characteristics of the designed adiabatic coupler. (a) Transmissions of the through and drop ports versus vertical gap spacing between the bus and coupler waveguides at 1550 nm wavelength, (b) spectral response of the drop port for various gap spacing. The designed adiabatic coupler exhibits broadband operation over a 300 nm wavelength range (1400–1700 nm).

switching operation. The transmissions at the drop and through ports were simulated for various gap spacings at a 1550 nm wavelength, as shown in Fig. 3(a). At the optimum spacing (125 nm), light is transmitted to the drop port with an optical loss of 0.01 dB. The transmission to the drop port decreases with increasing gap spacing, and the ON/OFF extinction ratio is larger than 45 dB at 800 nm gap spacing. In the ON state (125 nm gap spacing), the adiabatic coupler efficiently directs light to the drop port over a wavelength range of 300 nm (1400–1700 nm), as shown in Fig. 3(b). The adiabatic coupler has high tolerance to fabrication imperfections (Section III of Supplement 1).

3. EXPERIMENTAL RESULTS

Silicon photonic switches with 64 × 64 ports have been fabricated at Berkeley Marvell Nanofabrication Lab. The detailed fabrication process is described in Section IV of Supplement 1. The switch comprising 4096 switching cells has a footprint of 7 mm × 7 mm [Fig. 4(a)]. The area including all the input/output (I/O) couplers and routing waveguides is 8.6 mm × 8.6 mm. The close-up view of a unit cell (area = 110 μm × 110 μm) is shown in Fig. 4(b). Figures 4(c) and 4(d) show the scanning electron microscope (SEM) images of a perspective view of the switch array and a close-up view of a unit cell, respectively. The bus waveguides and the coupler waveguides are highlighted with red and blue colors, respectively, in Fig. 4(d). The coupler waveguide is suspended by micro springs at 1 μm above the bus waveguide in the OFF state. When the switch is turned on, the coupler waveguide is pulled down toward the bus waveguide by the MEMS actuator. The waveguide spacing in the ON state is precisely defined at 125 nm by mechanical stoppers, which are highlighted in Fig. 4(e). The SEM images of the couplers in the OFF and ON states are shown in Figs. 4(f) and 4(g), respectively.

To characterize the performance of the switches, TE-polarized light was coupled into the device using a 1 × 64 linear fiber array through grating couplers. The device has three arrays of 1 × 64 grating couplers, and each array connects 21 input ports, 21 through ports, and 20 output ports. The remaining two ports are connected back-to-back for optical alignment. The coupling loss of grating couplers was measured to be 6 dB from test

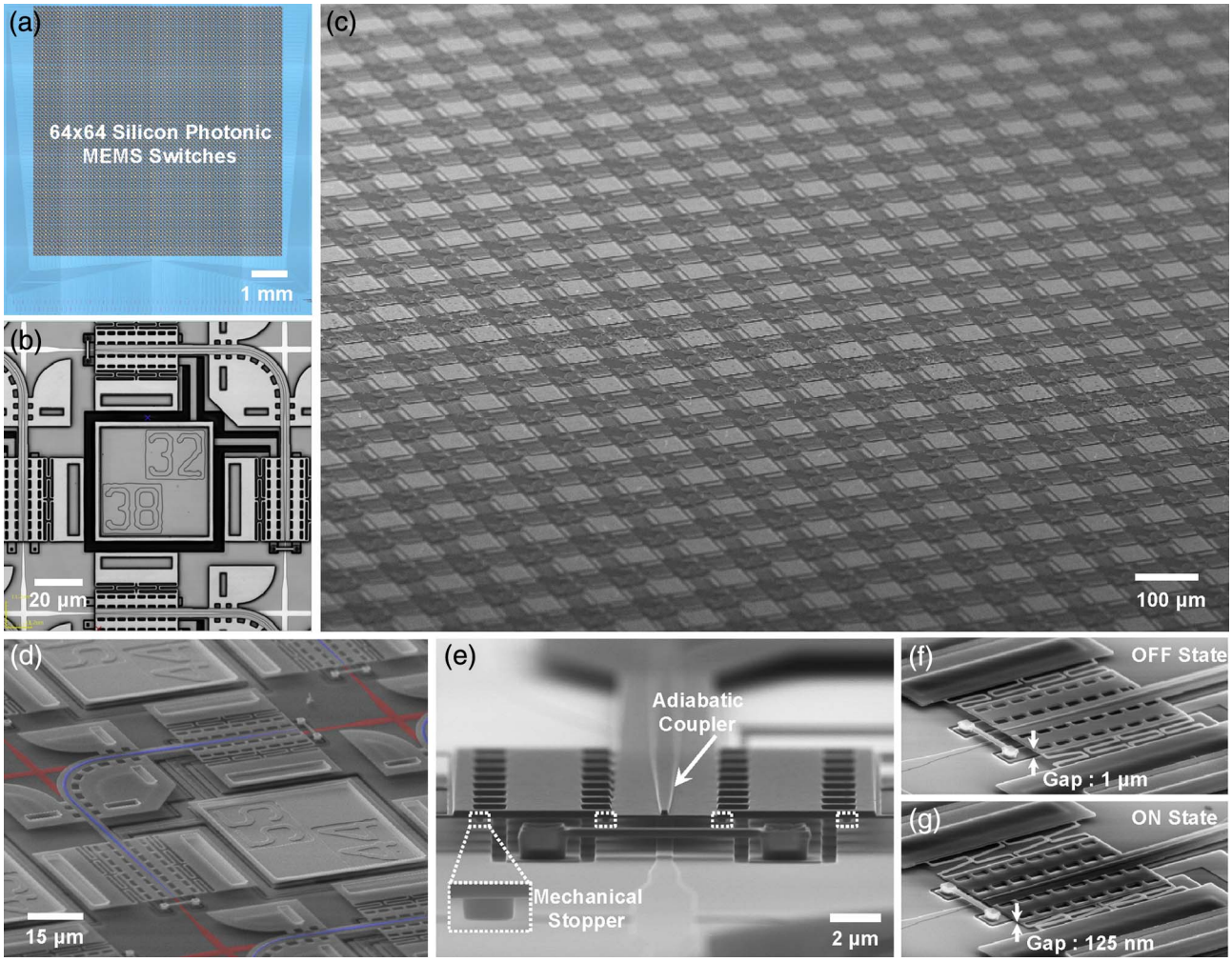

Fig. 4. Fabricated large-scale silicon photonic switches. (a) Microscope image of the fabricated device. A 64 × 64 silicon photonic switch array is integrated on an area of 7 mm × 7 mm. (b) Microscope image of a unit cell, (c) perspective SEM image of the fabricated silicon photonic switch array, (d) SEM image of a unit cell. Bus waveguides and coupler waveguides are highlighted with red and blue colors, respectively. (e) Close-up view SEM of the adiabatic coupler. The spacing between the bus and coupler waveguides is precisely defined by mechanical stoppers in the ON state. (f),(g) SEM images of the adiabatic couplers in (f) the OFF state and (g) the ON state.

structures on the same chip. The grating coupler for our measurement had not yet been optimized, and the use of tapered conical fibers can potentially reduce the I/O coupling loss to 0.13 dB [26]. The actuators in individual cells were electrically addressed using probe tips. Because the probing was manual, we limited our measurements to 172 randomly selected switching cells. In the selected cells all actuators operated without failure. Figure 5 shows the optical transmission of the drop port versus the applied voltage measured from a representative switching cell at a 1550 nm wavelength. The switch is turned on at 42 V and the optical power stays constant with further increase of the bias, which confirms the digital switching characteristics. It is well known that the gap-closing actuators exhibit bistable operation due to the nonlinear nature of the electrostatic force, which is inversely proportional to the square of the gap spacing [27]. Due to this bistable operation, the switch is turned on at "pull-in" voltage (42 V) and remains in the ON state until the voltage is reduced to 24 V. A large extinction (greater than 60 dB) is observed in the OFF state, which ensures light propagation through cells in the OFF state without disturbance. We also characterized the electrical cross talk by monitoring the optical power in adjacent drop ports when a switching cell was turned on. The optical power in the adjacent ports is below −60 dB, and there is no observable variation in power. We concluded that the electrical cross talk is very small.

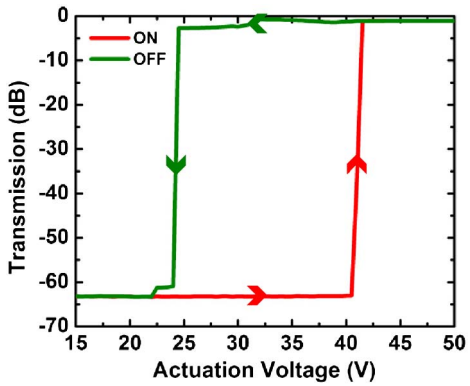

Fig. 5. Measured transfer characteristics as a function of actuation voltage. The digital switching characteristic is clearly observed.

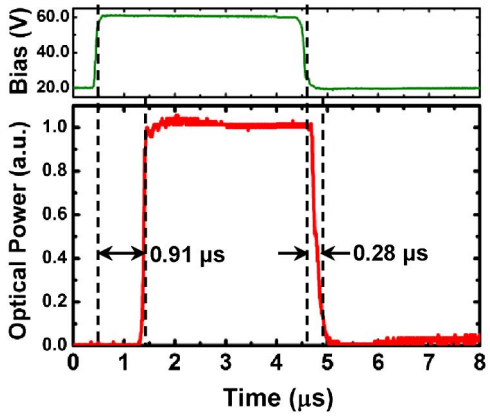

Fig. 6. Measured temporal response of a switch unit cell.

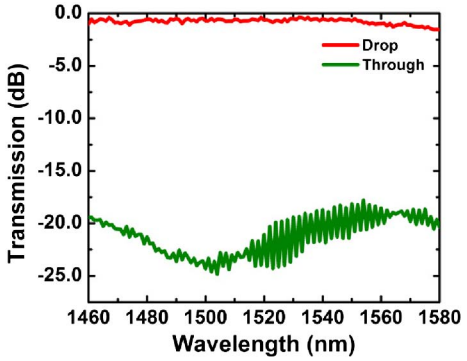

Fig. 8. Measured spectral response of a switch unit cell confirming broadband operation.

The temporal response of the switch was investigated by applying a step function of the bias voltage [Fig. 6]. The ON and OFF switching times were measured to be 0.91 and 0.28 μs, respectively, which are three orders of magnitude faster than conventional 2D or 3D MEMS switches [24]. The ON-switching time is longer than the OFF-switching time because the adiabatic couplers need to travel a distance of roughly 800 nm before initiating optical coupling. On the other hand, an initial coupler movement of 200 nm is sufficiently effective to turn off coupling, which results in the shorter OFF-switching time. The frequency response of the MEMS actuator was directly measured using a laser Doppler vibrometer, as shown in Fig. 7. The measured mechanical resonance frequency of 0.71 MHz agrees well with the switching times. To examine the spectral response of the switch, the transmissions of the drop and through ports in the ON state were recorded as the laser wavelength was tuned from 1460 to 1580 nm, the maximum range supported by our tunable laser. Broadband operation of the adiabatic couplers is clearly observed in Fig. 8.

The optical loss of our switch is mainly dominated by the propagation and the waveguide crossing losses as the switch size scales up. The propagation loss of the bus waveguide and the insertion loss of a single MMI crossing were measured to be 1.1 dB/cm and 0.017 dB/crossing, respectively, from passive test structures (Section V of Supplement 1). Based on these values, the estimated optical loss is 0.025 dB/cell. We also directly measured the insertion losses of 172 switching cells, including the one with the longest optical path. During this measurement, 14 input ports were selected and illuminated sequentially. The on-chip insertion losses were extracted by subtracting the 12 dB coupling loss. We plot the losses versus the number of cells in the light path in Fig. 9. The propagation loss (proportional to the number of cells) and the switching loss (fixed loss) can be extracted from the slope and the y intercept of the linear fitted line. The propagation loss is 0.026 dB/cell, which agrees well with the loss calculated from the passive test structures. The switching loss is estimated to be 0.47 dB. The maximum loss of the switch corresponding to the longest path is estimated to be 3.7 dB ($= 2 \times 63$ cells $\times$ 0.026 dB/cell + 0.47 dB).

To test the long-term reliability of the switch, we operated the switch over 10 billion cycles using a square wave voltage at 100 kHz. The optical transmissions in the ON and OFF states were measured every 10 million cycles [Fig. 10(a)]. No performance degradation was observed over the entire test period of 10^{10} cycles. Another possible failure mechanism is stiction after long physical contact in the ON state. We tested the switch with increasing time in the ON state and then measured optical transmissions in both ON and OFF states [Fig. 10(b)]. The switch successfully turned on and off for upto 48 h of continuous contact without any stiction observed. This reliability test was performed in ambient conditions without any packaging. It is expected that the long-term reliability is even better with hermetic packaging.

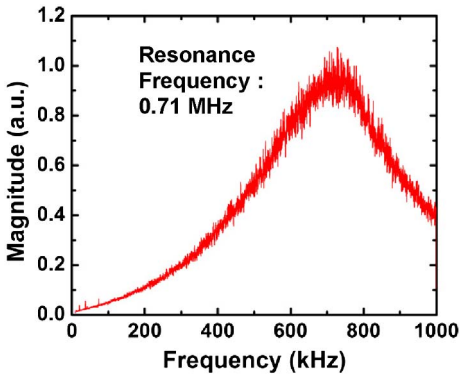

Fig. 7. Laser Doppler vibrometer measurement of a MEMS-actuated adiabatic coupler. The measured mechanical resonance frequency is 0.71 MHz.

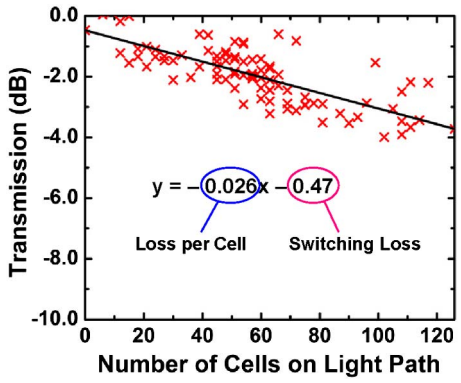

Fig. 9. On-chip insertion loss with various light paths. The passive loss per cell and switching loss are estimated to be 0.026 and 0.47 dB, respectively.

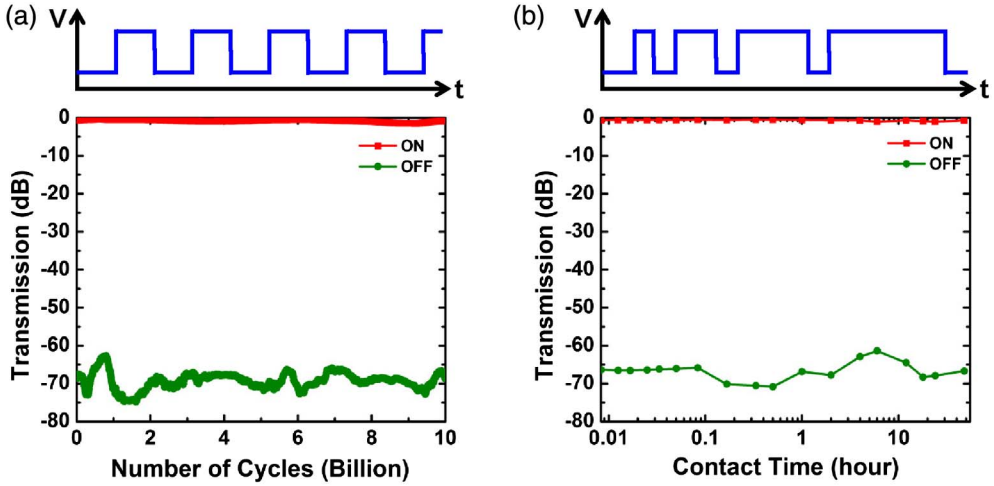

Fig. 10. Reliability test of the fabricated silicon photonic MEMS switch. (a) Repeatability test. The switch was turned on and off at 100 kHz, and the optical transmissions were measured every 10 million cycles. The switch successfully operated over 10 billion cycles without significant performance degradation. (b) Stiction test. The switch is held in the ON state continuously for various amount of time. No stiction was observed upto 48 h of contact time.

4. CONCLUSION

We have designed and experimentally demonstrated 64 × 64 silicon photonic switches with 3.7 dB on-chip losses, 0.91 μs switching times, digital operation, and broadband response from 1460 to 1580 nm (limited by the range of our tunable laser). The passive matrix architecture is (to our knowledge) fundamentally more scalable than other silicon photonic switches through its use of MEMS-actuated adiabatic couplers, which provide extremely high ON/OFF ratios and show essentially no loss in the OFF state. Light goes through the adiabatic couplers only once, irrespective of the size of the switch. Losses in the switch are presently dominated by those incurred in waveguide propagation and waveguide crossings. With an improved design and fabrication process, we foresee scaling the switch to several hundred ports while simultaneously reducing losses. In its present embodiment, our switch integrated 4096 MEMS-actuated adiabatic couplers on a 7 mm × 7 mm area. To our knowledge it is the largest silicon photonic integrated circuit thus far demonstrated.

Funding. National Science Foundation (NSF) (0939514, EEC-0812072); Defense Advanced Research Projects Agency (DARPA) (HR0011-11-2-0021).

See Supplement 1 for supporting content.

REFERENCES

1. L. Schares, X. J. Zhang, R. Wagle, D. Rajan, P. Selo, S.-P. Chang, J. R. Giles, K. Hildrum, D. M. Kuchta, J. L. Wolf, and E. Schenfeld, "A reconfigurable interconnect fabric with optical circuit switch and software optimizer for stream computing systems," in *Optical Fiber Communication Conference and National Fiber Optic Engineers Conference*, OSA Technical Digest (CD) (Optical Society of America, 2009), paper OTuA1.
2. G. Wang, D. G. Andersen, M. Kaminsky, K. Papagiannaki, T. S. E. Ng, M. Kozuch, and M. Ryan, "c-through: part-time optics in data centers," in *Proceedings of the ACM SIGCOMM Conference* (ACM, 2010), pp. 327–338.
3. A. Vahdat, H. Liu, X. Zhao, and C. Johnson, "The emerging optical data center," in *Optical Fiber Communication Conference/National Fiber Optic Engineers Conference*, OSA Technical Digest (CD) (Optical Society of America, 2011), paper OTuH2.
4. N. Farrington, A. Forencich, G. Porter, P.-C. Sun, J. E. Ford, Y. Fainman, G. C. Papen, and A. Vahdat, "A multiport microsecond optical circuit switch for data center networking," IEEE Photon. Technol. Lett. **25**, 1589–1592 (2013).
5. G. Porter, R. Strong, N. Farrington, A. Forencich, P. Chen-Sun, T. Rosing, Y. Fainman, G. Papen, and A. Vahdat, "Integrating microsecond circuit switching into the data center," in *Proceedings of the ACM SIGCOMM 2013 Conference* (ACM, 2013), pp. 447–458.
6. J. Bowers, A. Raza, D. Tardent, and J. Miglani, "Advantages and control of hybrid packet optical-circuit-switched data center networks," in *Advanced Photonics for Communications*, OSA Technical Digest (online) (Optical Society of America, 2014), paper PM2C.4.
7. B. G. Lee, N. Dupuis, P. Pepeljugoski, L. Schares, R. Budd, J. R. Bickford, and C. L. Schow, "Silicon photonic switch fabrics in computer communications systems," J. Lightwave Technol. **33**, 768–777 (2015).
8. D. Liang and J. E. Bowers, "Recent progress in lasers on silicon," Nat. Photonics **4**, 511-517 (2010).
9. G. T. Reed, G. Mashanovich, F. Y. Gardes, and D. J. Thomson, "Silicon optical modulators," Nat. Photonics **4**, 518–526 (2010).
10. M. Asghari and A. V. Krishnamoorthy, "Silicon photonics: energy-efficient communication," Nat. Photonics **5**, 268–270 (2011).
11. A. Rickman, "The commercialization of silicon photonics," Nat. Photonics **8**, 579–582 (2014).
12. P. P. Absil, P. Verheyen, P. De Heyn, M. Pantouvaki, G. Lepage, J. De Coster, and J. Van Campenhout, "Silicon photonics integrated circuits: a manufacturing platform for high density, low power optical I/O's," Opt. Express **23**, 9369–9378 (2015).
13. Y. Vlasov, W. M. J. Green, and F. Xia, "High-throughput silicon nanophotonic wavelength-insensitive switch for on-chip optical networks," Nat. Photonics **2**, 242–246 (2008).
14. J. Van Campenhout, W. M. Green, S. Assefa, and Y. A. Vlasov, "Low-power, 2 × 2 silicon electro-optic switch with 110-nm bandwidth for broadband reconfigurable optical networks," Opt. Express **17**, 24020–24029 (2009).
15. Y. Shoji, K. Kintaka, S. Suda, H. Kawashima, T. Hasama, and H. Ishikawa, "Low-crosstalk 2 × 2 thermo-optic switch with silicon wire waveguides," Opt. Express **18**, 9071–9075 (2010).
16. M. Yang, W. M. J. Green, S. Assefa, J. Van Campenhout, B. G. Lee, C. V. Jahnes, F. E. Doany, C. L. Schow, J. A. Kash, and Y. A. Vlasov, "Non-blocking 4 × 4 electro-optic silicon switch for on-chip photonic networks," Opt. Express **19**, 47-54 (2011).
17. A. V. Rylyakov, C. L. Schow, B. G. Lee, W. M. J. Green, S. Assefa, F. E. Doany, M. Yang, J. Van Campenhout, C. V. Jahnes, J. A. Kash, and Y. A. Vlasov, "Silicon photonic switches hybrid-integrated with CMOS drivers," IEEE J. Solid-State Circuits **47**, 345–354 (2012).

18. B. G. Lee, A. V. Rylyakov, W. M. J. Green, S. Assefa, C. W. Baks, R. Rimolo-Donadio, D. M. Kuchta, M. H. Khater, T. Barwicz, C. Reinholm, E. Kiewra, S. M. Shank, C. L. Schow, and Y. A. Vlasov, "Monolithic silicon integration of scaled photonic switch fabrics, CMOS logic, and device driver circuits," J. Lightwave Technol. **32**, 743–751 (2014).
19. S. Sohma, T. Watanabe, N. Ooba, M. Itoh, T. Shibata, and H. Takahashi, "Silica-based PLC type 32 × 32 optical matrix switch," in *European Conference on Optical Communications (ECOC)* (2006).
20. L. Chen and Y. Chen, "Compact, low-loss and low-power 8×8 broadband silicon optical switch," Opt. Express **20**, 18977-18985 (2012).
21. K. Suzuki, K. Tanizawa, T. Matsukawa, G. Cong, S.-H. Kim, S. Suda, M. Ohno, T. Chiba, H. Tadokoro, M. Yanagihara, Y. Igarashi, M. Masahara, S. Namiki, and H. Kawashima, "Ultra-compact 8 × 8 strictly-non-blocking Si-wire PILOSS switch," Opt. Express **22**, 3887–3894 (2014).
22. K. Tanizawa, K. Suzuki, M. Toyama, M. Ohtsuka, N. Yokoyama, K. Matsumaro, M. Seki, K. Koshino, T. Sugaya, S. Suda, G. Cong, T. Kimura, K. Ikeda, S. Namiki, and H. Kawashima, "Ultra-compact 32 × 32 strictly-non-blocking Si-wire optical switch with fan-out LGA interposer," Opt. Express **23**, 17599–17606 (2015).
23. S. Han, T. J. Seok, N. Quack, B.-W. Yoo, and M. C. Wu, "Large-scale silicon photonic switches with movable directional couplers," Optica **2**, 370–375 (2015).
24. M. C. Wu, O. Solgaard, and J. E. Ford, "Optical MEMS for lightwave communication," J. Lightwave Technol. **24**, 4433–4454 (2006).
25. V. Kaman, R. J. Helkey, and J. E. Bowers, "Compact and scalable three-dimensional microelectromechanical system optical switches," J. Opt. Netw. **6**, 19–24 (2007).
26. T. G. Tiecke, K. P. Nayak, J. D. Thompson, T. Peyronel, N. P. de Leon, V. Vuletić, and M. D. Lukin, "Efficient fiber-optical interface for nanophotonic devices," Optica **2**, 70–75 (2015).
27. J. G. Korvink and O. Paul, eds., *MEMS: A Practical Guide to Design, Analysis, and Applications* (William Andrew, 2006).